Physica Scripta

PAPER

# Study of optoelectronic and thermoelectric properties of double perovskites $X_2HfI_6$ (X = Ga, In, Tl) for renewable energy

**Nessrin A Kattan**[1], **Syed Awais Rouf**[2,*], **Q Mahmood**[3,4,*], **Murefah Mana AL-Anazy**[5], **Mohammed A Amin**[6], **H H Hegazy**[7,8], **Manal Morsi**[9,10], **Nouf H Alotaibi**[11] and **H H Somaily**[8]

[1] Department of Physics, College of Science, Taibah University, Medina, Saudi Arabia
[2] Department of Physics, Division of Science and Technology, University of Education, Lahore, Pakistan
[3] Basic and Applied Scientific Research Center, Imam Abdulrahman Bin Faisal University, PO Box 1982, Dammam, 31441, Saudi Arabia
[4] Department of Physics, College of Science, Imam Abdulrahman Bin Faisal University, PO Box 1982, Dammam, 31441, Saudi Arabia
[5] Department of Chemistry, College of Sciences, Princess Nourah bint Abdulrahman University (PNU), PO Box 84428, Riyadh, 11671, Saudi Arabia
[6] Department of Chemistry, College of Science, Taif University, PO Box 11099 Taif, 21944, Saudi Arabia
[7] Department of Physics, Faculty of Science, KingKhalid University, P.O. Box 9004, Abha, Saudi Arabia
[8] Research Center for Advanced Materials Science(RCAMS), King Khalid University, Abha 61413, P. O. Box 9004, Saudi Arabia
[9] Department of Physics, College of Arts and Science, Wadi Addawasir, Prince Sattam bin Abdulaziz University, Saudi Arabia
[10] Department of Physics, Girl Collage for Art, Science, and Education, Ain-Shams University, Cairo, Egypt
[11] Chemistry Department, College of Science, King Saud University, Riyadh 11451, Saudi Arabia
[*] Authors to whom any correspondence should be addressed.

**E-mail:** syedawais.rouf@ue.edu.pk **and** qmmustafa@iau.edu.sa

**RECEIVED**
3 August 2022

**REVISED**
19 February 2023

**ACCEPTED FOR PUBLICATION**
1 March 2023

**PUBLISHED**
20 March 2023

**Keywords:** density functional theory, optoelectronic devices, ultraviolet region of light energy, thermoelectric characteristics, high performance

## Abstract

The double perovskites (DPs) are outstanding materials for renewable energy and other optoelectronic applications. Here in this paper, the thermoelectric and optical behavior of $X_2HfI_6$ (X = Ga, In, Tl) have been explained systematically by DFT. The structural stability has been certified using ionic radii in terms of tolerance factor, and dynamic stability has been confirmed by positive phonon dispersion frequencies in acoustic modes. The band structure findings show the direct band gaps for (Ga, In, Tl) based DPs. The optical properties have been investigated by dispersion, absorption, refection, and related other optical characteristics. The absorption bands are existing in ultraviolet region and shifted to higher energy (blue shift). The reflection and optical loss of light are noted less than 0.3 which increases their potential for optoelectronic devices. The high Seebeck coefficient and electrical conductivity along with ultralow lattice thermal conductivity confirm the high figure of merit at and below the room temperature.

## 1. Introduction

The Increasing energy demand for sustainable development and industrialization has forced world policy makers to realize the usefulness of the alternative resources of energy [1]. In this regard, emphasis of researchers around the globe has been shifted towards the cause of fulfilling the energy needs of humans. The most easily accessible and ideal source of renewable energy is the Sunlight which is not only cheap but also reliable. In recent past, many scientists have discovered efficient and cheap solar cell materials that largely exploit the visible spectrum [2]. Another source for renewable energy is the change of heat energy to beneficial electrical energy via electrical generators. The figure of merit $ZT = \sigma S^2/\kappa T$ has been used to determine performance of thermoelectric devices which largely depends upon electrial conductivity and Seebeck coefficient. The most excellent thermoelectric compounds should have high $\sigma$ and S but must have small $\kappa$ [3]. The efficiency of devices developed for renewable energy depends upon the selection of compounds.

Recently, power conversion efficiency (PCE) of about 25.6% has been achieved for lead-based double perovskite halides that are potential candidates for solar cells production [3–5]. In 2019, Geisz *et al* [6] described

the solar cell efficiency of 47.1% by multi-junction concentrator solar cells, i.e., 11.1% higher than that of earlier reported efficiency. Kojima *et al*, reported $CH_3NH_3PbI_3$ ($MAPbI_3$) perovskite solar cells have limited practical applications because they show poor stability due to decomposition of $CH_3NH_3PbI_3$ into $CH_3NH_3I$, $PbI_2$ and $I_2$ due to ambient conditions and toxic nature of Pb [7, 8]. It has been observed that in all inorganic perovksites, the method of ion exchange has improved the stability of perovskite solar cells (PSCs) expressively [9, 10]. That's why, finding new halide perovskites is very important for green energy. Many researchers have found several stable halide perovskites as shown in [11–17].

Recently, double perovskites of type $A_2B(I)B(III)X_6$, which were obtained after modifiying divalent B(II) cation into monovalent B(I) and trivalent B(III) cations, overcome issue of instability [18]. The $Cs_2AgBiX_6$ [X = Br, Cl] double perovskite halides were first time made by solid-state and solution method [19, 20]. Furthermore, $A_2BX_6$ materials have been made by exchanging B-site cation in $A_2B(I)B(III)X_6$ double perovskites with some vacancy order element [21]. Compounds like $A_2BX_6$ and $ABX_3$ are of alike structures having closed pack behaviour, for example, $Cs_2SnI_6$, $Cs_2PdBr_6$, and $Cs_2TeI_6$ etc [22–26]. Numerous investigations about halide perovskites including experimental [26] and theoretical [27] have been carried out to recognize the ideal materials. These materials have excellent structural, electronic, optical, and thermoelectric behaviour [28].

The light absorption within visible and infrared regions has been studied for $A_2BX_6$ (where B = Sn and Te) compounds that make them potential materials for optoelectronic devices [29, 30]. The determined values of band gap are in the range from 1.25 eV to 1.30 eV for $Cs_2SnI_6$ that was obtained from diffuse-reflectance studies [31, 32]. It present a new highly stable perovskite $Cs_2PdBr_6$ having band gap 1.60 eV for PScs usage. The n-type semiconducting nature of $Cs_2PdBr_6$ was confirmed from the calculated effective masses of electron and hole having value of 0.53 $m_e$ and 0.85 $m_e$, respectively [33]. The experimental and theoretical investigations about $A_2TiX_6$ , where $A = K^+$, $Rb^+$, $Cs^+$, and $In^+$; X = Cl, Br, and I) and $Cs_2TiI_xBr_{6-x}$ have been presented. The band gaps from 1.38 eV to 1.78 eV fall absorption in the visible region and highlight the perovskites as an excellent materials for photovoltaic devices. It was further stated [34] that all these halide perovskites are stable, however the $Rb_2TiI_6$ and $Cs_2TiI_6$ are most stable compounds because $\Delta H > 50$ meV/atom. Researchers have also performed computational investigations of few known materials having form $A_2BX_6$ (where A = K, Rb, and Cs, B = Sn, Pd, Pt, Te, and X = I) with HSE06 functional [35]. It was reported that the band gap values and the effective masses of these materials increases by changing A-site cation from K to Rb to Cs.

From the experimental and theoretical literature of the family of these materials, the cubic phase of the studied double perovskites has been analyzed. For example, Hakami explored the $A_2ZrI_6$ (A = Ga, In and Tl) in cubic phase with space group Fm $\bar{3}$ m by DFT based codes and ensured their stability in cubic phase by tolerance factor, and positive frequencies of phonon dispersion [36]. Vuong *et al*, studied the $Tl_2HfCl_6$ by experimental approach and analyzed by x-ray diffraction which the cubic phase with space group Fm $\bar{3}$ m [37]. Moreover, Hawrami *et al*, studied the Intrinsic Tl/Hf/Zr-based scintillators of double perovskites $Tl_2HfCl_6$ and $Tl_2ZrCl_6$ in cube phase [38]. In addition to the above, the family compounds of the studied double perovskites are vastly studied in the materials project [39]. Therefore, in the knowledge of above discussion, we have explored the studied double perovskites for optical and thermoelectric applications because these properties are not yet explained.

We have studied $X_2HfI_6$ (X = Ga, In, Tl), a novel double perovskites iodides which have limited experimental and/or theoretical data. The structral, dynamic and thermodynamic confirmation by tolerance factor, formation energy and phonons dispersion analysis ureged us to explore them for optoelectronic and thermoelectric applications. Furthermore, the large figure of meritand Seebeck coefficent are also make them promising mateirals for direct conversion of heat energy into electrical energy. To the best of our knowledge, we have comprehensively studied optical and thermoelectric properties of these materials for the very first time. Thus, our predictions offer profound opportunity to the experimentalists to investigate them for useful applications.

## 2. Methods of calculation

The DPs $A_2H_fI_6$ (A = Ga, In, Tl) are studied for electronic and optical characteristics by using Wien2k software [40] which based on full potential linearized augmented plane wave FP-LAPW method [37]. The Perdew–Burke–Ernzerhof generalized-gradient approximation PBE-GGA [41] is used to calculate the precise results of ground state characteristics, i.e., lattice constant, bulk modulus, and bandgap. It fails to calculate the band gap of these materials accurately. Therefore, modified Becke and Johnson potential of Tran and Blaha (TB-mBJ) [42] has been applied that calculate value of band gap accurately. We have used $R_{MT} \, x \, K_{max} = 8$, $G_{max} = 20$ $(Ry)^{1/2}$, and $l_{max} = 10$. The, 12 × 12 × 12 k-mesh is used to achieve convergence of charge/energy. For optical and thermoelectric properties, the K-mesh has been increased 20 × 20 × 20 to make it dense. The maximum convergence threshold for energy/charge is fixed at $10^{-4}$ Ry. The optical characteristics have been evaluated

using Krammer-Kronge expression [43, 44] that linked the real and imaginary parts as

$$\varepsilon_1(\omega) = 1 + \frac{2}{\pi} P \int_0^{\infty} \frac{\omega' \varepsilon_2(\omega')}{\omega'^2 - \omega^2} d\omega' \tag{1}$$

$$\varepsilon_2(\omega) = \frac{e^2 h'}{\pi m^2 \omega^2} \sum_{v,c} \int_{BZ}^{\infty} |M_{cv}(k)|^2 \delta[\omega_{cv}(k) - \omega] d^3k \tag{2}$$

The thermoelectric characteristics of DPs are computed by BoltzTraP code [45]. The transport coefficient of $\sigma$ are given as

$$\sigma_{\alpha\beta}(\varepsilon) = \frac{1}{N} \sum_{i,k} \sigma_{\alpha\beta}(i, k) \frac{\delta(\varepsilon - \varepsilon_{i,k})}{\delta(\varepsilon)} \tag{3}$$

$$\sigma_{\alpha\beta}(i, k) = e^2 \tau_{i,k} \upsilon_{\alpha}(i, \vec{k}) \upsilon_{\beta}(i, \vec{k}) \tag{4}$$

Here wave number is N, relaxation time is $\tau$, and group velocity is $\upsilon_{\beta}$. Moreover, Seebeck coefficient and electrical conductivity as a function of temperature and chemical potential can be written in integral form as

$$\sigma_{\alpha\beta}(\alpha, \mu) = \frac{1}{\Omega} \int \sigma_{\alpha\beta}(\varepsilon) \left[ -\frac{\partial f_0(T, \varepsilon, \mu)}{\partial \varepsilon} \right] d\varepsilon \tag{5}$$

$$S_{\alpha\beta}(T, \mu) = \frac{1}{eT\Omega\sigma_{\alpha\beta}(T, \mu)} \int \sigma_{\alpha\beta}(\varepsilon)(\varepsilon - \mu) \left[ -\frac{\partial f_0(T, \varepsilon, \mu)}{\partial \varepsilon} \right] d\varepsilon. \tag{6}$$

The values of $\sigma$ and S tells us about the greater efficiency of thermoelectric devices having low thermal conductivity. Furthermore, the phonons calcutions and lattice thermal conductiity are calculated by phonopy code [45] and ShengBTE code [46]

## 3. Results and discussion

### 3.1. Structural and electronic properties

The DPs $X_2HfI_6$ (X = Ga, In, Tl) having face-centered cubic (FCC) structure which belong to Fm $\overline{3}$ $m$ space group. The geometrical structure is given in figure 1(A), in which $X_2HfI_6$ (X = Ga, In, Tl) consist of $HfI_6$ octahedra groups. All individual octahedra $HfI_6$ are parted from other octahedra through 12-fold coordinates of iodine. The vacant positions among these octahedra $HfI_6$ are occupied by Ga/In/Tl. It can be seen from figure 1(A) that the Hf and Ga/In/Tl are bounded by 6- and 12-iodine ions, respectively. The bond length Hf-I reduces due to the strong coordination in $X_2HfI_6$ (X = Ga, In, Tl). Therefore, each $HfI_6$ is positioned at the center and corners of the cubic structure. The Ga/In/Tl, Hf, and I are located at 8c, 4a, and 24e Wyckoff sites fractional coordinates [47]. The optimized positions of two atoms of Ga/In/Tl, one atom of Hf and 6 atoms of I are as In (0.25, 0.25, 0.25), In (0.75, 0.75, 0.75), Hf (0, 0, 0), I (0.25, 0, 0), I (0.75, 0, 0), I (0, 0.25, 0), (0, 0.75, 0), I (0, 0, 0.25), and ( 0, 0, 0.75). The $Ga_2HfI_6$ has lattice constant of 12.52 Å and rises to 12.56 Å due to the change of Ga with In and Tl, as In (265 pm) and Tl (300 pm) has a larger atomic size as compare to Ga (243 pm) whereas decrease in the bulk modulus is given in table 1. The energy versus volume plots of studied DPs show the complete optimization and relaxation of the structures as depicted in figure 1(B). The increasing or decreasing of lattice constant depends upon the matching of radii of cations and anions. In the present case, the atomic radius increases from Ga to Tl which increasing the matching of their radii with Hf and In. Therefore, the lattice constant decreases and band gap increases from Ga to Tl substitution. The elements X, Hf, and I in the formula $X_2HfI_6$ have the oxidation states +1, +4 and -1, respectively which balanced the charge as [(+1 × 2) + (+4 × 1) + (-1 × 6)]. These are the similar oxidation states as occurs in $Cs_2SnI_6$ as +1, +4 and -1 for Cs, Sn, and I, respectively. Usually, the Ga/In/Tl have oxidation states +3 but it also attains +1 in many mechanisms. In literature, the scientists have elaborated +1-oxidation state of Ga/In/Tl in $In_2O$ [48] which is further explained by Zhao *et al*, and Schneider *et al* [49, 50].

The studied DPs are found thermodynamically stable and is clarified from calculating the formation energy

$$\Delta H_f = E_{Total}(X_l Hf_m I_n) - lE_X - mE_{Hf} - nE_I \tag{7}$$

Where $E_{Total}(X_l Hf_m I_n)$ is total energy of materials, and $E_X$, $E_{Hf}$ and $E_I$ are energies of individual atoms. The calculated formation energies are listed in table 1, whose negative values confirms that studied DPs are thermodynamically stable [51]. The structural stability is confirmed from Goldschmidt formula

$$t = (r_X + r_I)/\sqrt{2}\,(r_{Hf} + r_I) \tag{8}$$

Where $r_X$, $r_{Hf}$ and $r_I$ are ionic radii of X, Hf and I, respectively [52]. For cubic DPs to be a stable structure, the ideal tolerance factor is unity. The structural stability of studied DPs is confirmed from computed values given in table 1. The octahedral factor or ionic ratio $\mu = r_{Hf}/r_I$, where $r_{Hf}$ and $r_I$ are the ionic radii of Hf and I ions are

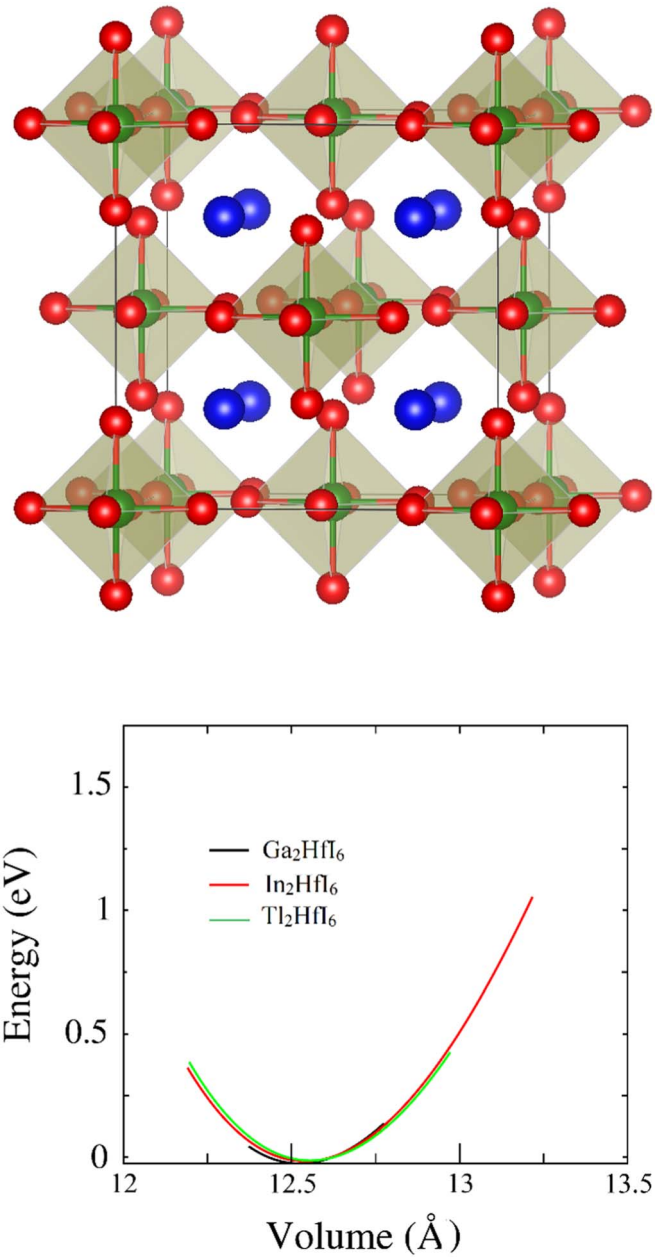


**Figure 1.** (A) Crystal structures of $X_2HfI_6$ (X = Ga, In, Tl); [Red color of I, Blue color of Hf, Green color of Ga, In, Tl]. Figure 1(B) energy versus volume plots $X_2HfI_6$, (X = Ga, In, Tl).

**Table 1.** The calculated parameters for $Ga_2HfI_6$, $In_2HfI_6$, and $Tl_2HfI_6$.

| Parameter | $Ga_2HfI_6$ | $In_2HfI_6$ | $Tl_2HfI_6$ |
|---|---|---|---|
| Lattice constant $a_o$(Å) | 12.52 | 12.54 | 12.56 |
| Bulk modulus $B_o$ (*GPa*) | 17.62 | 17.34 | 17.30 |
| Formation energy $H_f$ (eV) | −2.95 | −2.65 | −2.45 |
| Band gap $E_g$(eV) | 2.70 | 2.75 | 2.90 |
| Tolerance factor $T_f$ | 0.89 | 0.90 | 0.92 |
| Octahedral factor ($\mu$) | 0.44 | 0.45 | 0.47 |
| Static refractive index $n(0)$ | 1.90 | 2.00 | 1.83 |
| Static dielectric constant $\varepsilon_1(0)$ | 3.63 | 4.07 | 3.36 |
| Reflectivity $R(0)$ | 0.097 | 0.114 | 0.086 |

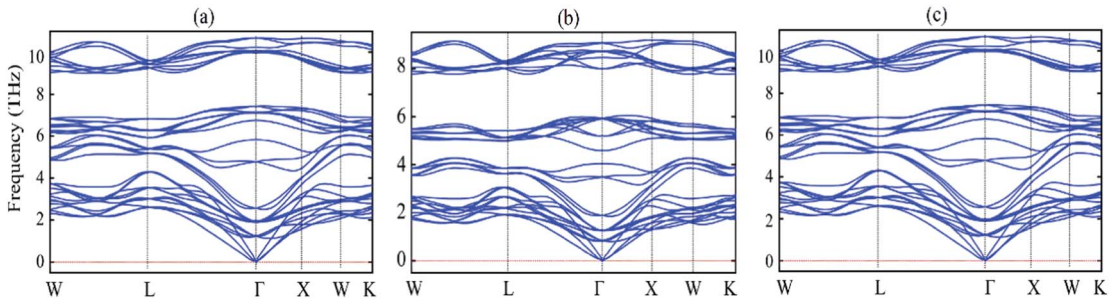


**Figure 2.** The phonons disperson plots of (a) $Ga_2HfI_6$, (b) $In_2HfI_6$, and (c) $Tl_2HfI_6$.

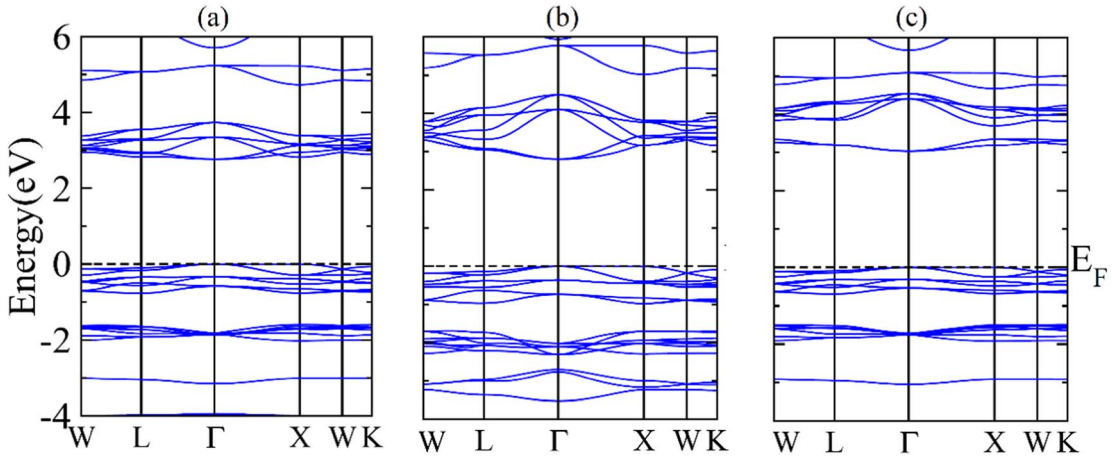


**Figure 3.** Band structures of (a) $Ga_2HfI_6$, (b) $In_2HfI_6$, and (c) $Tl_2HfI_6$.

calculated for the studied double perovskites. Our computed values 0.44, 0.45 and 0.47 are falls in the stability range 0.42 to 0.68. Moreover, our findings are consistent with calculations in the [53]. These values of octahedral factor are also presented in table 1.

Furthermore, for dynamic stability confirmation which is very important for device formation, the phonons dispersion calculations are executed by phonopy code and depicted in figures 2(a)–(c). There are two modes of phonons are observed optical mode at frequency and acoustic mode at low frequency. The optical modes have positive frequencies and show the stable behavior. The acoustic mode of phonons are also meet at Γ direction to zero frequecy of their 3 phonons [54, 55]. Therefore, during the analysis of phonons band structures the negative frequecies are not present which ensure the dynamic stabilities of studied DPs.

The electronic performance of studied DPs is elaborated by band structures (BS) whose graphs are plotted in figures 3(a)–(c). The electronic configurations of atoms are Ga [Ar] $3d^{10}$ $4s^2$ $4p^1$, In [Kr] $4d^{10}$ $5s^2$ $5p^1$, Tl [Xe] $4f^{14}$ $5d^{10}$ $6s^2$ $6p^1$, Hf [Xe] $4f^{14}$ $5d^2$ $6s^2$, and I [Kr] $4d^{10}$ $5s^2$ $5p^5$. The valence electrons contribute to the transitions across the band gap and physical properties of the materials. Here the Ga, In, and Tl have one electron in the $4p^1$, $5p^1$, and $6p^1$, respectively. The Hf and I have two electrons in $5d^2$ and five electrons in $5p^5$. Therefore, we have plotted only the Ga ($4p^1$), In ($5p^1$), Tl ($6p^1$), Hf ($5d^2$) and I ($5p^5$) states and ignore the rest of states. In the figure 3, we have only written as Ga/In/Tl p-states, Hf d-states and I p-states. The valence band exist at Fermi level for the analyzed DPs, which ensures the states in the VB below $E_F$ are occupied. Moreover, maxima of VB at and minima of CB at Γ direction show the direct band gap of studied DPs which increases by changing Ga with In and Tl which is may be due to addition of extra states in the tetrahedral positions. In addition, the density of states under the $E_F$ in VB are richer than the DOS in the CB, therefore, the effective mass ($m^*$) of holes VB are larger than electrons in the CB. The $m^*$ are for electrons ($m_e^*$) and holes ($m_h^*$) are computed from BS at Γ-L-1,2 and Γ-X-1 directions (See table 2) [56]. The calculated values of $m_e^*$ and $m_h^*$ are consistent with BS (See figure2). The holes have larger $m_h^*$ as compared to $m_e^*$ which can also be seen from flat DOS at VB in BS plots. These effective masses largely effect the physical properties especially thermoelectric properties which are discussed in the last section of article. The effective masses are used in transport properties calculations such as electrons and holes when they move under the influence of field and density of states of carriers in semiconductors. The large

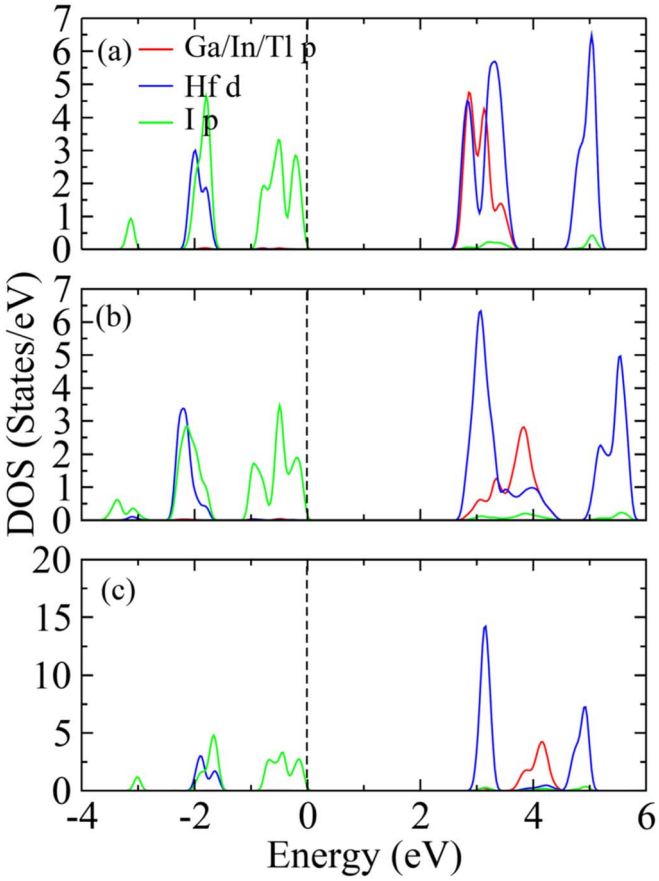


**Figure 4.** DOS of Ga/In/Tl, Hf, and I for (a) $Ga_2HfI_6$, (b) $In_2HfI_6$, and (c) $Tl_2HfI_6$.

**Table 2.** Computed effective masses of electrons ($m_e^*$) and holes ($m_h^*$).

| Direction | $Ga_2HfI_6$ | | $In_2HfI_6$ | | $Tl_2HfI_6$ | |
|---|---|---|---|---|---|---|
| | $m_h^*$ | $m_e^*$ | $m_h^*$ | $m_e^*$ | $m_h^*$ | $m_e^*$ |
| (Γ-L)-1 | 3.99 | 2.20 | 2.98 | 1.80 | 4.11 | 3.00 |
| (Γ-L)-2 | 2.45 | 2.28 | 2.00 | 1.83 | 2.55 | 2.92 |
| (Γ-X)-1 | >10 | 3.21 | >10 | 3.14 | >10 | 4.03 |
| (Γ-X)-2 | 1.60 | 1.42 | 1.20 | 1.02 | 1.64 | 1.53 |

values of carrier's effective masses reduce the electrical conductivity and increases the Seebeck coefficient. Therefore, the vacancy ordered double perovskites have large values of Seeback coefficient as measured in the present in mV/K and consistent with the results measured in the [36]. The effective masses also decide the behavior of band structures, for heavy carriers the density of states becomes flat while for light effective masses the states are curved. Large values of effective also influence the transition and recombination rate of the carriers.

The valence DOS of studied DPs for Ga/In/Tl, Hf and I are drawn in figures 4(a)–(c). Therefore, Ga/In/Tl have the valence orbitals 4p/5p/6p, and Hf/I have 5d/5p orbitals. In the VB, the energy regions -1.6 to -2.1 eV and zero to -1.0 eV contains the p states of I. The d states of Hf lies at -1.7 to -2.1 eV in the VB while d states of Hf in CB lies at energy 2.6 to 3.8 eV and 4.6 to 5.5 eV along with the p states of Ga/In/Tl in the energy region 2.6 to 3.8 eV. Theretofore, the pd hybridization of I-Hf and X-Hf in the CB control the possible transitions and recombination's between VB and CB. The favorable transitions go on from the p states of I in VB to d states of Hf in CB.

### 3.2. Optical properties

The optical behavior depends upon light–matter interaction which is measured by dielectric constant $\varepsilon(\omega)$ who's real $\varepsilon_1(\omega)$ and imaginary $\varepsilon_2(\omega)$ parts represents the dispersion of light energy and absorption. The $\varepsilon_1(\omega)$ and $\varepsilon_2(\omega)$ are related through Kramer-Kronig relations whose expressions are given in [57–59]. For studied DPs, the

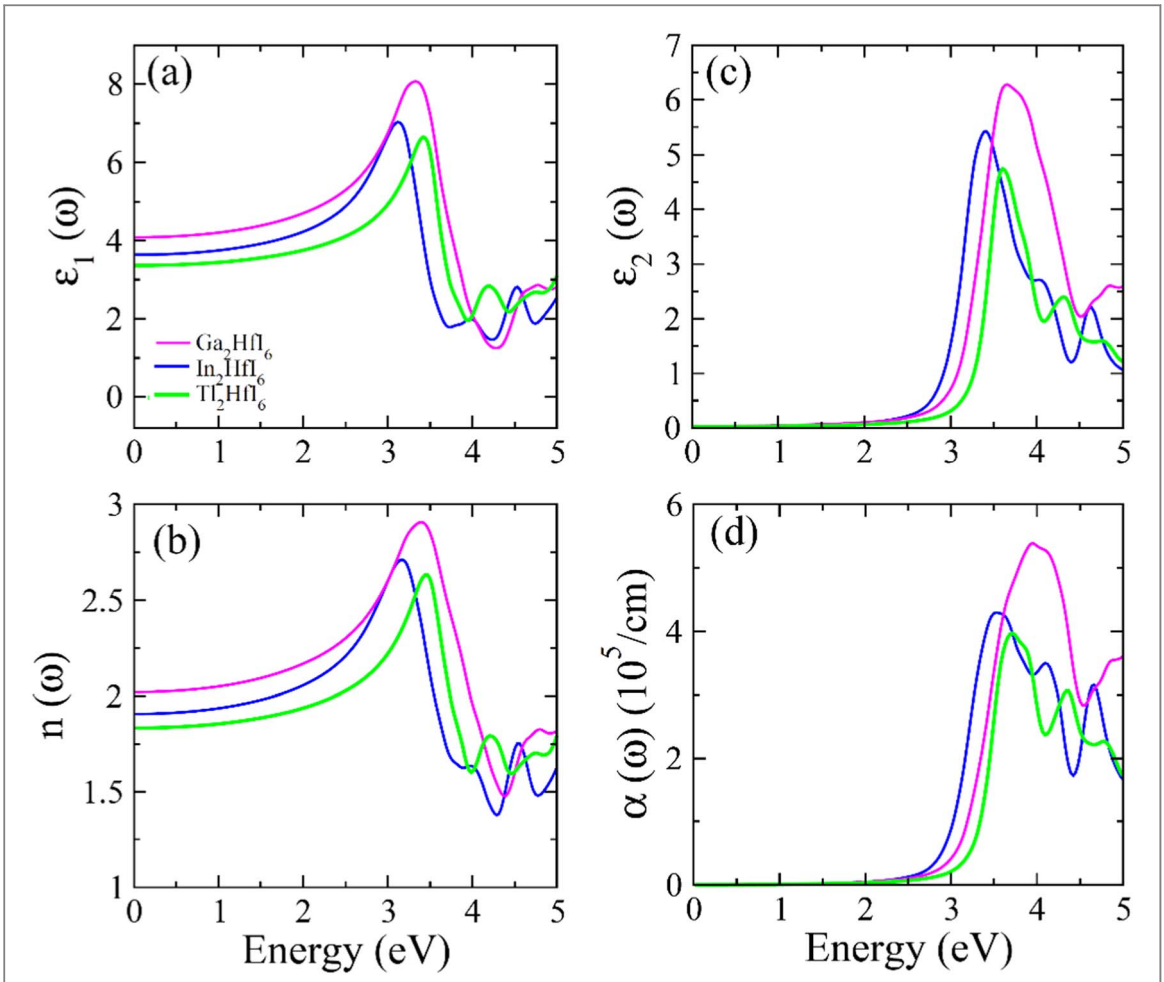


**Figure 5.** Dielectric constnats (a) $\varepsilon_1(\omega)$, (b) refractive index n ($\omega$) (c), $\varepsilon_2(\omega)$, and (d) absorption $\alpha(\omega)$ $Ga_2HfI_6$, $In_2HfI_6$, and $Tl_2HfI_6$.

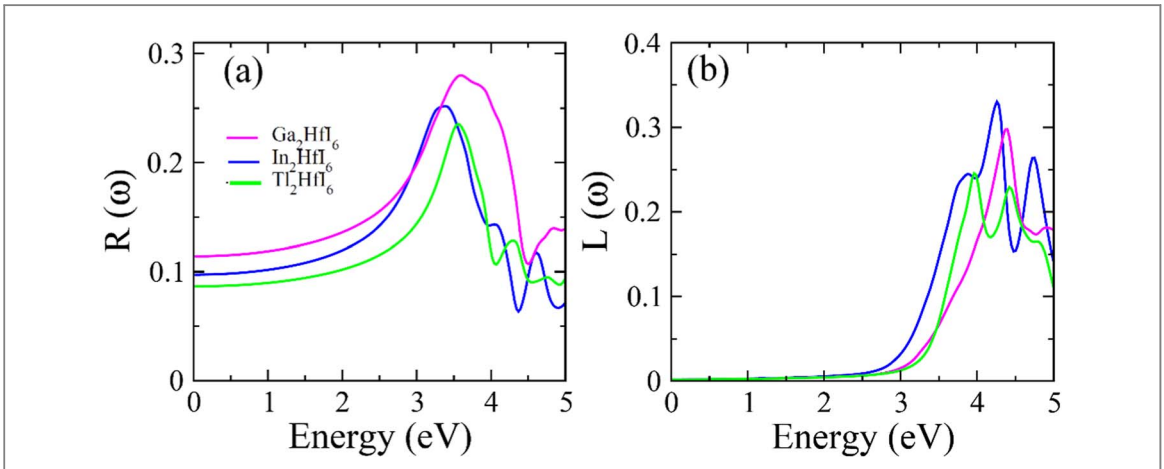


**Figure 6.** (a) R($\omega$) and (b) L($\omega$) of $A_2HfI_6$ (A = Ga, In, Tl).

calculated optical parameters are shown in figures 5(a)–(d) and 6(a), (b). The $\varepsilon_1(\omega)$ accounts for the polarization caused by the electromagnetic waves while passing through materials [60]. It has been noticed from figure 5(a) that $\varepsilon_1(\omega)$ increases with increasing in light intensity and show peaks at 3.4 eV (8.0), 3.2 eV (7.0), and 3.5 eV (6.5) for $Ga_2HfI_6$, $In_2HfI_6$, and $Tl_2HfI_6$, respectively. after resonance, $\varepsilon_1(\omega)$ begins to fall, and its values stay positive for all our studied compounds which confirm their semiconducting nature.

The static dielectric constants and optical band gaps are agree with Penn's model expressed as $\varepsilon_1(0) \approx 1 + (\hbar\omega_p/E_g)^2$ [61], here $E_g$, $\hbar$, and $\omega_p$ are optical band gap, Planck's constant, and plasma frequency, respectively (See table 1). The n($\omega$) informs us about the inclination of materials to be transparent and computed values are

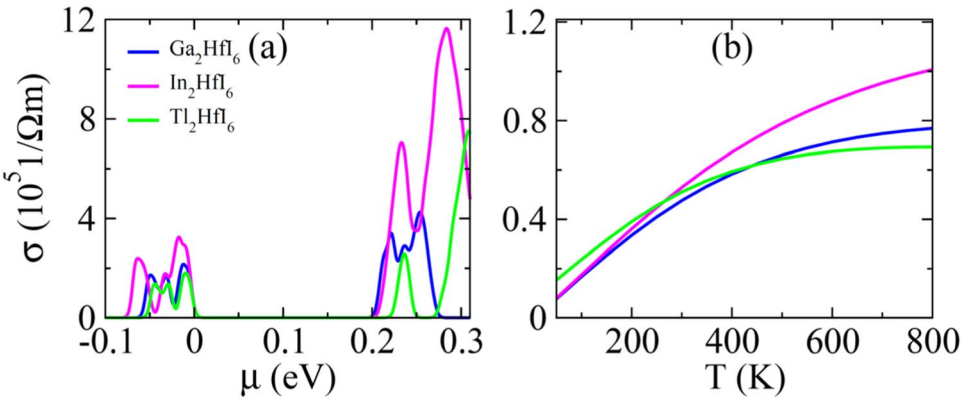


**Figure 7.** The $\sigma$ versus (a) $\mu$ and (b) T for $X_2HfI_6$ (X = Ga, In, Tl).

plotted in figure 5(b). The static refractive index $n$ (0) for $Ga_2HfI_6$, $In_2HfI_6$, and $Tl_2HfI_6$ relate to $\varepsilon_1(0)$ through relation $n_0^2 = \varepsilon_1(0)$ [62] as given in table1. It has been noted that $\varepsilon_1(\omega)$ and $n(\omega)$ values changes consistently. Its main values appear at 3.4 eV (2.90), 3.2 eV (2.75), and 3.5 eV (2.60), and then becomes least as drawn in figure 5(b).

The light energy absorbed by optical compounds is found from $\varepsilon_2(\omega)$ as presented in figure 5(c). As seen from figure 5(c), $\varepsilon_2(\omega)$ reaches to highest values at 3.6 eV (6.5), 3.4 eV (5.5), and 3.5 eV (4.8), after that drops to small value due to various transition and recombination rates. The absorption bands appeared at (2.8 to 4.4) eV, (2.7 to 3.8) eV, and (3.2 to 4.0) eV for $Ga_2HfI_6$, $In_2HfI_6$, and $Tl_2HfI_6$, respectively. These values of band gaps and absorption bands pointed out that studied compounds have worth in visible, and ultraviolet region. The $\alpha(\omega)$ has similar trends as $\varepsilon_2(\omega)$ because both demonstrate light absorption. The $\alpha(\omega)$ is shown in figure 5(d) for $Ga_2HfI_6$, $In_2HfI_6$, and $Tl_2HfI_6$ which have peak values at 4.0 eV, 3.4 eV, and 3.5 eV, respectively.

The reflectivity R($\omega$) is plotted in figure 6(a) and its values at zero frequency are presented in table 1 which are extremely low. The observed peak values of reflectivity are 0.28, 0.25, and 0.24 for $Ga_2HfI_6$, $In_2HfI_6$, and $Tl_2HfI_6$, respectively. The loss energy L($\omega$) is drawn in figure 6(b). The observed L($\omega$) has small value in the visible and ultraviolet regions. Therefore, the R($\omega$) and L($\omega$) are very small in visible to ultraviolet regions which make them promise for energy applications.

### 3.3. Thermoelectric properties

The transport behavior of DPs $Ga_2HfI_6$, $In_2HfI_6$, and $Tl_2HfI_6$ is mainly depends upon S, $\sigma$ and $\kappa$ which are computed by BoltzTraP code. Therefore, the ($\sigma$, S, $\kappa$) are addressed thoroughly to ensure the performance of studied DPs in terms of figure of merit ZT ($\sigma S^2/\kappa$) [63–66]. For the finest thermoelectric materials, the ZT must be high for which the $\sigma/\kappa$ and S should be large. The $\kappa$ consists of lattice vibration ($\kappa_{ph}$) and electrons motion ($\kappa_e$) which moves through materials in terms waves of energy. In present study, the $\kappa_e$ only computed classical Boltzmann theory for thermoelectric performance. However, in the late section the $\kappa_{ph}$ is computed separately and discussed. For complete understanding of carrier's concertation and behavior of thermoelectric parameters are focused by temperature (T) and chemical potential ($\mu$) in figures 7–12. The S, $\sigma$, and $\kappa$ versus chemical potential at room temperature 300 K. The $\mu$ discriminates the electrons (n-type) and holes (p-type) carriers by its positive and negative values. The most important factor is the relaxation time ($\tau$) time which is considered average of collisions in the studied system as $10^{-14}$s for $\sigma$ and $\kappa$.

The figure 7(a) show from zero to -0.07 eV the $\sigma$ has intensity below $3.6 \times 10^5$ (1/ Ωm) while in the n-type site the large intensities $4.0/11.9/7.8 \times 10^5$ (1/ Ωm) for Ga/In/Tl based DPs are found in the energy range 0.2 to 0.3 eV. Therefore, it is observed the $In_2HfI_6$ has highest intensity for the studied DPs with majority carriers' electrons. Furthermore, the $\sigma$ has values $0.1 \times 10^5$ (1/ Ωm) for Ga/In and $0.15 \times 10^5$ (1/ Ωm) for Tl at 50 K as depicted in figure 7(b). The increases temperature enhances their $\sigma$ and it becomes $0.79/0.78/0.9 \times 10^5$ (1/ Ωm) for Ga/In/Tl based DPs at 800 K, respectively.

The $\kappa_e$ has similar trends as $\sigma$ as depicted in figure 8(a) because we are considering only electronic its electronic part. It has values 1.2/2.2/1.1 W/mK for Ga/In/Tl based DPs, respectively in the energy zero to -1.0 eV in p-type side. While in n-type side the it has values 2.5/8.0/4.5W/mK for Ga/In/Tl based DPs. For temperature range from zero to 800 K, its values increase to 1.6/2.6/1.3 W/mK for Ga/In/Tl based DPs, respectively (See figure 8(b)). The value of $\sigma$ is $10^5$ time larger than $\kappa$ which increase the significant for thermoelectric applications [66, 67].

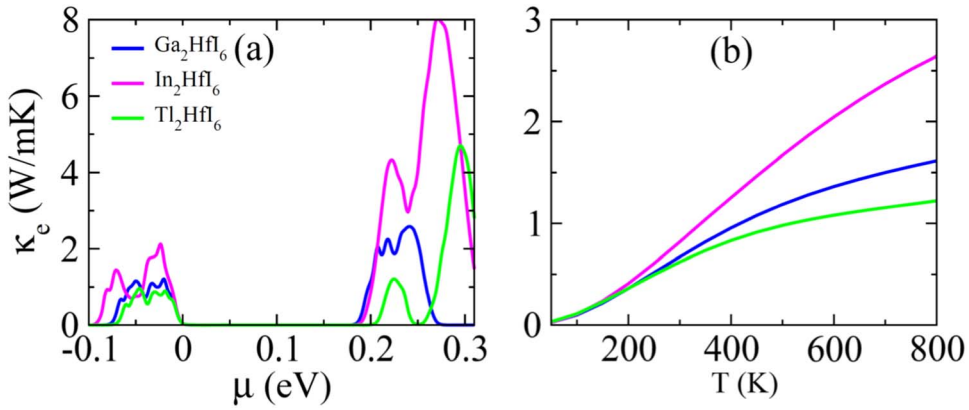


**Figure 8.** The $\kappa_e$ versus (a) $\mu$ and (b) T for $X_2Hfl_6$ (X = Ga, In, Tl).

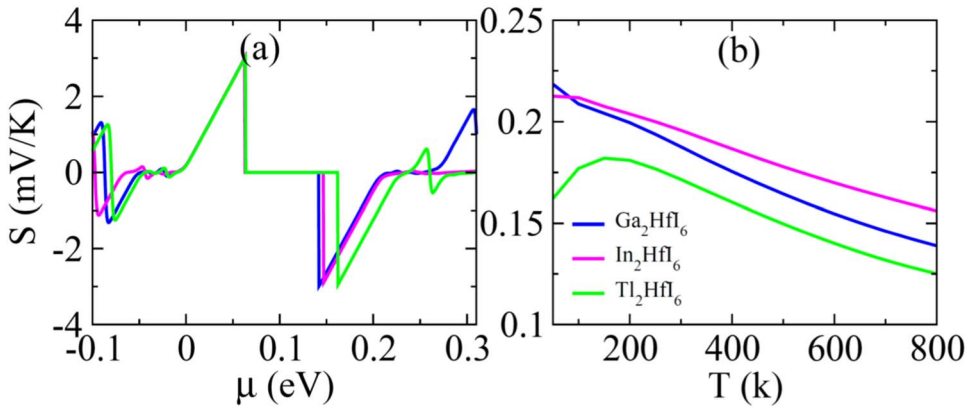


**Figure 9.** The S versus (a) $\mu$ and (b) T for $A_2Hfl_6$ (A = Ga, In, Tl).

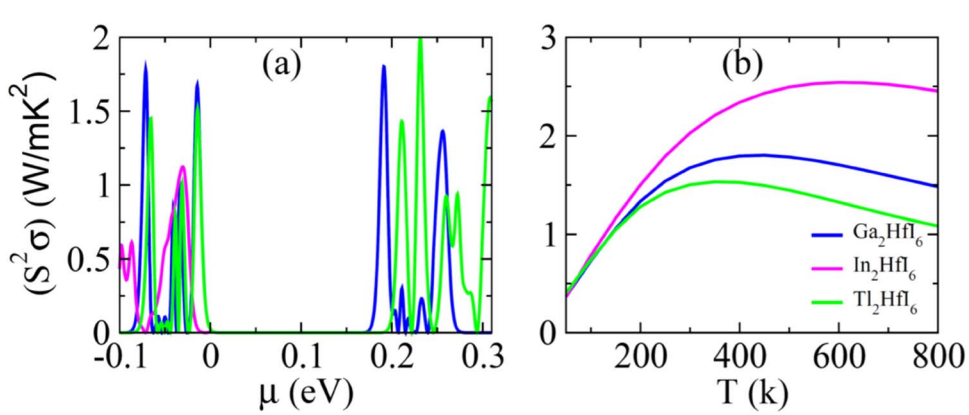


**Figure 10.** The PF versus (a) $\mu$ and (b) T for $A_2Hfl_6$ (A = Ga, In, Tl).

The S is the difference of potential according to temperature between two contact of metals and play a leading role to increase the thermoelectric performance of the device. Its negative values refer to electrons and positive values refer to holes as main source of carriers. The calculated S against $\mu$ has been displayed in figure 9(a) which show its values reaches to positive peak at 0.06 eV and negative peak at 0.14/16 eV for Ga/In/Tl based DPs with peak intensity $\pm 3$ mV/K. The fluctuation also occurs at $-0.9$ eV in the p-type region but its intensity is very small. The S is also plotted versus T and noted its values are 0.23/0.22 mV $K^{-1}$ at 50 K and then decreases linearly for Ga, and In based DPs up to 0.13/0.16 mV $K^{-1}$ at 800 K (See figure 9(b)). For $Tl_2Hfl_6$ its value first increases up to 200 K and then decreases to 0.13 mV $K^{-1}$ at 800 K.

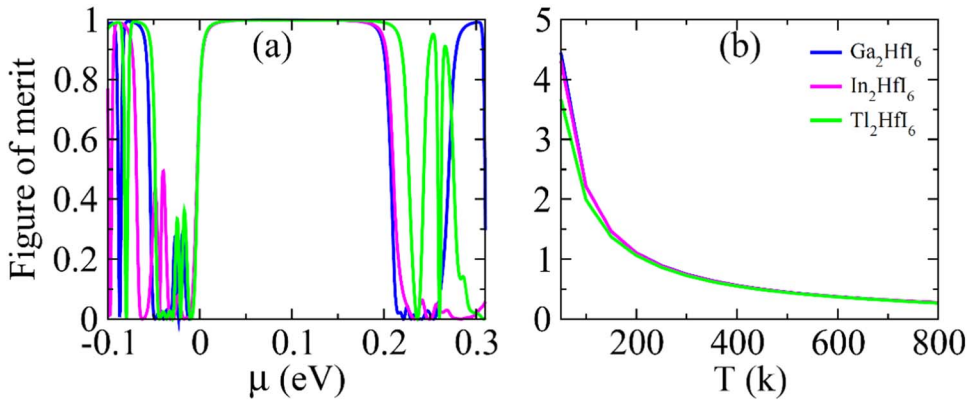


**Figure 11.** The ZT versus (a) $\mu$ and (b) T for $A_2HfI_6$ (A = Ga, In, Tl).

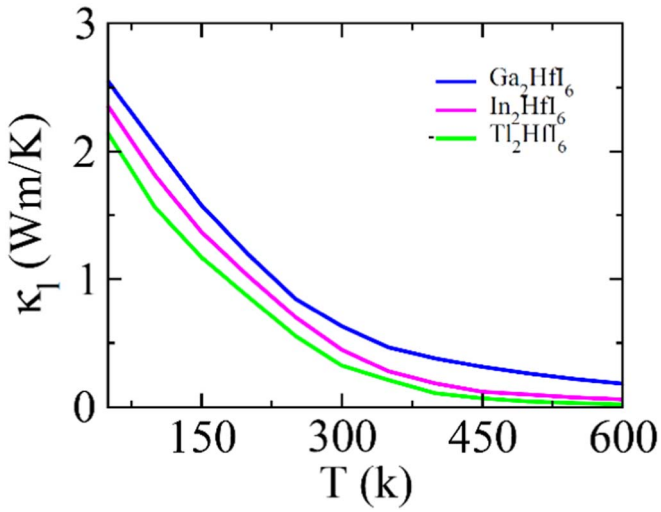


**Figure 12.** The $\kappa_L$ versus T for $A_2HfI_6$ (A = Ga, In, Tl).

The $S^2\sigma$ is measured as power factor of thermoelectric materials which decides about the performance. The computed values are illustrated in figure 10(a) against $\mu$ which show in the p-type side from zero -0.1 eV the hole carriers have significant contribution for Ga/In/Tl based DPs. On the other side, the electrons have contribution in the energy region from 0.17 to 0.30 eV for Ga and Tl. The behavior of PF against T has been plotted in figure 10(b) whose values are 0.9 W $mK^{-2}$ at 50 K. It increases to linearly up to 2.5/1.5/1.1 W $mK^{-2}$ at 800 K for Ga/In/Tl based DPs.

The ZT values decides the materials for thermoelectric devices and their efficiencies [68]. Therefore, the calculated ZT are depicted in figure 11(a) for $\mu$. In the energy range -0.1 eV to zero in p-type side and from 0.2 to 0.3 eV for n-type side the carriers support fully to ZT to improve the performance. At the Zero energy edge favor contributor is Tl based DPs and at 0.2 eV the Ga/In based DPs. However, the ZT behavior versus T in the range zero to 800 K shows the ZT is high (4.5, 4.4, 3.8) for (Ga, In, Tl) at 50 K and it decreases with rising T (See figure 11(b)). It becomes 0.8 at the room temperature (300 K) which further decreases to 0.3 at 800 K for studied DPs. Therefore, the large values of ZT at low T even at room temperature make them significant for thermoelectric applications.

Finally, to see the contribution of lattice vibration, the $\kappa_\ell$ has been plotted in figure 12, its value is ultralow which do not affect the performance of the thermoelectric devices. The computed values are compared with existing literature like GeTe, PbTe, $PbSe_{0.5}Te_{0.5}$ and $Bi_2Te_3$ have $\kappa_\ell$ values 2.60 W $mK^{-1}$, 2.0 W $mK^{-1}$, 1.50 W $mK^{-1}$ and 1.24 W $mK^{-1}$, respectively [69–72]. The other most relevant thermoelectric players are $X_2GeI_6$

(X = K, Rb, Ge) and $Cs_2PdI_6$ have $\kappa_\ell$ values 0.11/0.13/0.17 W mK$^{-1}$, and 0.15 W mK$^{-1}$ with large figure of merit [73].

## 4. Conclusion

The Pb free DPs are outstanding materials for optoelectronic and renewable energy applications. Here the computed findings ensure the positive phonon frequencies in acoustic mode, negative formation energy and tolerance factor (0.90 to 1.04) confirm their dynamic, thermal, and structural stabilities. The band gaps computed from BS ensures their applications for optoelectronic in visible to ultraviolet regions. The absorption bands from 2.8 to 3.5 eV was observed by imaginary dielectric constant and absorption coefficient which are most suitable optoelectronic devices especially light emitting diodes. The reflection and optical loss of light energy is less than 0.3 which is very significant factor. Lastly, the large values of ($\sigma$, S) and small values of $\kappa$ make the ZT significant (0.80) at room temperature. The ultralow $\kappa_l$ confirm was found for the studied DPs with is consistent with best thermoelectric players. Therefore, our significant findings of optoelectronic and thermoelectric characteristics will provide guidance to experimental researchers to realize them for applications.

## Acknowledgments

This research was funded by the Princess Nourah bint Abdulrahman University Researchers Supporting Project number (PNURSP2023R7), Princess Nourah bint Abdulrahman University, Riyadh, Saudi Arabia. The authors gratefully thank the Deanship of Scientific Research at King Khalid University for funding this work through the Small Groups Project under grant number (R.G.P.1/67/43).

## Data availability statement

The data cannot be made publicly available upon publication because the cost of preparing, depositing and hosting the data would be prohibitive within the terms of this research project. The data that support the findings of this study are available upon reasonable request from the authors.

## Conflict of interest

The author declares no competing financial interests [31].

## ORCID iDs

Syed Awais Rouf https://orcid.org/0000-0002-8508-2572

## References

[1] Ajia I A, Edwards P R, Liu Z, Yan J C, Martin R W and Roqan I S 2014 Excitonic localization in AlN-rich $Al_xGa_{1-x}N/Al_yGa_{1-y}N$ multi-quantum-well grain boundaries *Appl. Phys. Lett.* **105** 122111
[2] Lorenz K, Miranda S M C, Alves E, Roqan I S, O'Donnell K P and Boćkowski M 2012 High pressure annealing of europium implanted GaN *Gallium Nitride Materials and Devices VII* **8262** 82620C
[3] Eperon G E *et al* 2016 Perovskite-perovskite tandem photovoltaics with optimized band gaps *Science* **354** 861–5
[4] Alaal N and Roqan I S 2018 Tuning the electronic properties of hexagonal two-dimensional GaN monolayers via doping for enhanced optoelectronic applications *ACS Appl. Nano Mater.* **2** 202–13
[5] Zhou L, Xu Y F, Chen B X, Kuang D B and Su C Y 2018 Synthesis and photocatalytic application of stable lead-free $Cs_2AgBiBr_6$ perovskite nanocrystals *Small* **14** 1703762
[6] Geisz J F, Steiner M A, Jain N, Schulte K L, France R M, McMahon W E, Perl E E and Friedman D J 2018 Building a six-junction inverted metamorphic concentrator solar cell *IEEE J. Photovolt.* **8** 626–32
[7] Li Z Z, Xu Q C, Sun Q D, Hou Z F and Yin W J 2019 Thermodynamic stability landscape of halide double perovskites via high-throughput computing and machine learning *Adv. Funct. Mater.* **29** 1807280
[8] Zhang Y Y, Chen S Y, Xu P, Xiang H, Gong X G, Walsh A and Wei S H 2018 Intrinsic instability of the hybrid halide perovskite semiconductor $CH_3NH_3PbI_3$ *Chin. Phys. Lett.* **35** 036104
[9] Zelai T, Rouf S A, Mahmood Q, Bouzgarrou S, Amin M A, Aljameel A I, Ghrib T, Hegazy H H and Mera A 2022 *J. Mater. Resch. Techn* **16** 631–9
[10] Jiang J, Jiang J, Onwudinanti C K, Hatton R A, Bobbert P A and Tao S 2018 Stabilizing lead-free all-inorganic tin halide perovskites by ion exchange *J. Phys. Chem. C* **122** 17660–7
[11] Saliba M *et al* 2016 Incorporation of rubidium cations into perovskite solar cells improves photovoltaic performance *Science* **354** 206–9
[12] Stoumpos C C, Cao D H, Clark D J, Young J, Rondinelli J M, Jang J I, Hupp J T and Kanatzidis M G 2016 Ruddlesden-popper hybrid lead iodide perovskite 2D homologous semiconductors *Chem. Mater.* **28** 2852–67

[13] Chen P, Bai Y, Wang S C, Lyu M Q, Yun J H and Wang L Z 2018 *In Situ* growth of 2D perovskite capping layer for stable and efficient perovskite solar cells *Adv. Funct. Mater.* **28** 1706923
[14] Fan J D, Ma Y P, Zhang C L, Liu C, Li W Z, Schropp R E I and Mai Y H 2018 Thermodynamically self-healing 1D-3D hybrid perovskite solar cells, advanced energy *Materials* **8** 1703421
[15] Chen H N, Xiang S S, Li W P, Liu H C, Zhu L Q and Yang S H 2018 Inorganic perovskite solar cells: a rapidly growing field *Sol. RRL* **2** 23
[16] Xiao Z G, Zhao L F, Tran N L, Lin Y, Silver S H, Kerner R A, Yao N, Kahn A, Scholes G D and Rand B P 2017 Mixed-halide perovskites with stabilized bandgaps *Nano Lett.* **17** 6863–9
[17] Luo P F, Zhou S W, Zhou Y G, Xia W, Sun L, Cheng J G, Xu C X and Lu Y W 2017 Fabrication of $Cs_xFA_{1-x}PbI_3$ mixed-cation perovskites via gas-phase-assisted compositional modulation for efficient and stable photovoltaic devices *ACS Appl. Mater. Interfaces* **9** 42708–16
[18] Wang Z P, McMeekin D P, Sakai N, van Reenen S, Wojciechowski K, Patel J B, Johnston M B and Snaith H J 2017 Efficient and air-stable mixed-cation lead mixed-halide perovskite solar cells with n-doped organic electron extraction layers *Adv. Mater.* **29** 8
[19] McClure E T, Ball M R, Windl W and Woodward P M 2016 $Cs_2AgBiX_6$ (X = Br, CI): new visible light absorbing, lead-free halide perovskite semiconductors *Chem. Mater.* **28** 1348–54
[20] Absike H, Baaalla N, Lamouri R, Labrim H and Ez-zahraouy H 2022 Optoelectronic and photovoltaic properties of $Cs_2AgBiX_6$ (X = Br, Cl, or I) halide double perovskite forsolar cells: Insight from density functional theory *Int. J. Energy. Research* **46** 11053–64
[21] Slavney A H, Hu T, Lindenberg A M, Karunadasa H I and Bismuth-Halide A 2016 Double perovskite with long carrier recombination lifetime for photovoltaic applications *JACS* **138** 2138–41
[22] Maughan A E, Ganose A M, Bordelon M M, Miller E M, Scanlon D O and Neilson J R 2016 Defect tolerance to intolerance in the vacancy-ordered double perovskite semiconductors $Cs_2SnI_6$ and $Cs_2TeI_6$ *JACS* **138** 8453–64
[23] Jodlowski A D, Rodriguez-Padron D, Luque R and de Miguel G 2018 Alternative perovskites for photovoltaics, advanced energy *Materials* **8** 24
[24] Sakai N, Haghighirad A A, Filip M R, Nayak P K, Nayak S, Ramadan A, Wang Z P, Giustino F and Snaith H J 2017 Solution-processed cesium hexabromopalladate(IV), $Cs_2PdBr_6$, for optoelectronic applications *JACS* **139** 6030–3
[25] Neukom M, Zufle S, Jenatsch S and Ruhstaller B 2018 Opto-electronic characterization of third-generation solar cells *Sci. Technol. Adv. Mater.* **19** 291–316
[26] Hernandez-Haro N, Ortega-Castro J, Martynov Y B, Nazmitdinov R G and Frontera A 2019 DFT prediction of band gap in organic-inorganic metal halide perovskites: an exchange-correlation functional benchmark study *Chem. Phys.* **516** 225–31
[27] Yue S Y, Zhang X L, Qin G Z, Yang J Y and Hu M 2016 Insight into the collective vibrational modes driving ultralow thermal conductivity of perovskite solar cells *Physical Review B* **94** 115427
[28] Zhao T Q, Wang D and Shuai Z G 2017 Doping optimization of organic-inorganic hybrid perovskite $CH_3NH_3PbI_3$ for high thermoelectric efficiency *Synth. Met.* **225** 108–14
[29] Lee B, Stoumpos C C, Zhou N J, Hao F, Malliakas C, Yeh C Y, Marks T J, Kanatzidis M G and Chang R P H 2014 Air-stable molecular semiconducting Iodosalts for solar cell applications: $Cs_2SnI_6$ as a hole conductor *JACS* **136** 15379–85
[30] Saparov B, Sun J P, Meng W W, Xiao Z W, Duan H S, Gunawan O, Shin D, Hill I G, Yan Y F and Mitzi D B 2016 Thin-film deposition and characterization of a sn-deficient perovskite derivative $Cs_2SnI_6$ *Chem. Mater.* **28** 2315–22
[31] Chung I, Song J H, Im J, Androulakis J, Malliakas C D, Li H, Freeman A J, Kenney J T and Kanatzidis M G 2012 $CsSnI_3$: semiconductor or metal? High electrical conductivity and strong near-infrared photoluminescence from a single material. high hole mobility and phase-transitions *JACS* **134** 8579–87
[32] Zhao X G, Yang D W, Ren J C, Sun Y H, Xiao Z W and Zhang L J 2018 Rational design of halide double perovskites for optoelectronic applications *Joule* **2** 1662–73
[33] Ju M G, Chen M, Zhou Y Y, Garces H F, Dai J, Ma L, Padture N P and Zeng X C 2018 Earth-abundant nontoxic titanium(IV)-based vacancy-ordered double perovskite halides with tunable 1.0 to 1.8 eV bandgaps for photovoltaic applications *ACS Energy Lett.* **3** 297–304
[34] Ju M G, Chen M, Zhou Y, Garces H F, Dai J, Ma L, Padture N P and Cheng Zeng X 2018 *ACS Energy Lett.* **3** 297–304
[35] Cai Y, Xie W, Ding H, Chen Y, Thirumal K, Wong L H, Mathews N, Mhaisalkar S G, Sherburne M and Asta M 2017 Computational study of halide perovskite-derived $A_2BX_6$ inorganic compounds: chemical trends in electronic structure and structural stability *Chem. Mater.* **29** 7740–9
[36] Hakami O 2022 *Study of New Inorganic Double Perovskites Iodides $A_2ZrI_6$ (A = Ga, In, Tl) for Solar Cells and Renewable Energy* **46** 11326–35
[37] Vuong P Q, Tyagi M, Kim S H and Kim H J 2019 Crystal growth of a novel and efficient $Tl_2HfCl_6$ scintillator with improved scintillation characteristics *CrystEngComm* **21** 5898–904
[38] Hawrami R, Ariesanti E, Buliga V, Burger A, Lam S and Motake S 2020 $Tl_2HfCl_6$ and $Tl_2ZrCl_6$: Intrinsic Tl-, Hf-, and Zr-based scintillators *J. Crystal Growth* **531** 125316
[39] Jain A *et al* 2013 The materials project: a materials genome approach to accelerating materials innovation *APL Mater.* **1** 011002
[40] Schwarz K, Blaha P and Madsen G K H 2002 Electronic structure calculations of solids using the WIEN2k package for material sciences *Comput. Phys. Commun.* **147** 71–6
[41] Blaha P, Schwarz K, Madsen G K H, Kvasnicka D and Luitz J 2016 Wien2K code, an augmented plane wave plus local orbitals program for calculating crystal properties (Vienna, Austria: Vienna University of Technology)
[42] Perdew J P, Ruzsinszky A, Csonka G I, Vydrov O A, Scuseria G E, Constantin L A, Zhou X and Burke K 2008 Restoring the density-gradient expansion for exchange in solids and surfaces *Phys. Rev. Lett.* **100** 136406
[43] Tran F and Blaha P 2009 Accurate band gaps of semiconductors and insulators with a semilocal exchange-correlation potential *Phys. Rev. Lett.* **102** 226401–4
[44] Jiang S *et al* 2016 Pressure-dependent polymorphism and bandgap tuning of methyl ammonium lead iodide perovskites *Angew. Chem. Int. Ed.* **55** 6540
[45] Madsen G K H and Singh D J 2006 BoltzTraP. A code for calculating band-structure dependent quantities *Comput. Phys. Commun.* **175** 67–71
[46] Togo A and Tanaka I 2015 First principles phonon calculations in materials science *Scr. Mater.* **108** 1–5
[47] Li W, Carrete J, Katcho N A, Mingo N and BTE S 2014 A solver of the boltzmann transport equation for phonons *Comput. Phys. Commun.* **185** 1747–58
[48] Xiao Z, Lei H, Zhang X, Zhou Y, Hosono H and Kamiya T 2015 Ligand-hole in $[SnI_6]$ unit and origin of band gap in photovoltaic perovskite variant $Cs_2SnI_6$ *Bull. Chem. Soc. Jpn.* **88** 1250–5
[49] Tuck D G 1993 The lower oxidation states of indium *Chem. Soc. Rev.* **22** 269–76
[50] Schneider U and Kobayashi S 2012 Low-oxidation state indium-catalyzed C-C bond formation *Acc. Chem. Res.* **45** 1331–44

[51] Zhao Y X, Yuan K, Lia M Y and Zhao X 2020 Oxidation states of gallium (infrequent i and common iii) tunable via medium-sized C60 and small-sized C28 fullerenes *Inorg. Chem. Front.* **7** 4113–7
[52] Sabir B, Murtaza G, Mahmood Q, Ahmad R and Bhamu K C 2017 First principles investigations of electronics, magnetic, and thermoelectric properties of rare Earth based $PrYO_3$ (Y = Cr, V) perovskites *Current Appl. Phys.* **17** 1539–46
[53] Boubchir M, Boubchir R and Aourag H 2021 The use of principal component analysis for the prediction of double halide perovskites $A_2BX_6$ *J. Multiscale Modelling* **12** 2150004
[54] Mahmood Q, Haq B U, Yaseen M, Ramay S M, Ashiq M G B and Mahmood A 2019 The first-principle study of mechanical, optical, and thermoelectric properties of $SnZrO_3$ and $SnHfO_3$ for renewable energy applications *Solid State Commun.* **292** 17–23
[55] Jong U G, Yu C J and Kye Y H 2020 Computational prediction of structural, electronic, and optical properties and phase stability of double perovskites $K_2SnX_6$ (X = I, Br, Cl) *RSC Adv.* **10** 201
[56] Jong U G, Yu C J, Kye Y H, Choe S H, Kim J S and Choe Y G 2019 Anharmonic phonons and phase transitions in the vacancy-ordered double perovskite $Cs_2SnI_6$ from first-principles predictions *Phys. Rev. B* **99** 184105
[57] Al-Muhimeed T I, Shafique A, AlObaid A A, Morsi M, Nazir G, AL-Anazy M M and Mahmood Q 2021 *New Lead-Free Double Perovskites $X_2GeI_6$ (X = K, Rb, Cs) for Solar Cells, and Renewable Energy as an Alternate Of Hybrid Perovskites* **45** 19645–52
[58] Roqan I S, O'Donnell K P, Martin R W, Edwards P R, Song S F and Vantomme A 2010 Identification of the prime optical center in GaN: $Eu^{3+}$ *Physical Review B* **81** 085209
[59] Cai Y, Xie W, Ding H, Chen Y, Thirumal K, Wong L H, Mathews N, Mhaisalkar S G, Sherburne M and Asta M 2017 Computational study of halide perovskite-derived $A_2BX_6$ inorganic compounds: chemical trends in electronic structure and structural stability *Chem. Mater.* **29** 7740–9
[60] Hassan M, Arshad I and Mahmood Q 2017 Semicond. computational study of electronic, optical, and thermoelectric properties of $X_3PbO$ (X = Ca, Sr, Ba) anti-perovskites *Sci. Technol.* **32** 115002
[61] Haq B U, AlFaify S, Laref A, Ahmed R, Butt F K, Chaudhry A R, Ur Rehman S and Mahmood Q 2019 Optoelectronic properties of new direct bandgap polymorphs of single-layered Germanium sulfide *Ceram. Int.* **45** 18073–8
[62] Penn D R 1962 Wave-number-dependent dielectric function of semiconductors *Phys. Rev.* **128** 2093
[63] Dolling G, Enkrich C, Wegener M, Soukoulis C M and Linden S 2006 Simultaneous negative phase and group velocity of light in a metamaterial *Science* **312** 892–4
[64] Sajjad M, Singh N and Larsson J A 2020 Bulk, and monolayer bismuth oxyiodide (BiOI): Excellent high temperature p-type thermoelectric materials *AIP Adv.* **10** 075309
[65] Flemban T H, Singaravelu V, Devi A A S and Roqan I S 2015 Homogeneous vertical ZnO nanorod arrays with high conductivity on an *in situ* Gd nanolayer *RSC Adv.* **5** 94670–8
[66] Singh D, Sajjad M, Larsson J A and Ahuja R 2020 Promising high-temperature thermoelectric response of bismuth oxybromide *Results in Physics* **19** 103584
[67] Khan T. T and Chul U S 2018 Thermoelectric properties of the perovskites-type oxide $SrTi_{1-x}Nb_xO_3$ synthesized by solid-state reaction method *Electron. Mater. Lett.* **14** 336–41
[68] Oyama T, Muta H, Uno M and Yamanaka S 2004 Thermoelectric properties of perovskites type barium molybdate *J. Alloys. Compounds* **372** 65–9
[69] Nazir G, Rehman A, Hussain S, Algrafy E, Mahmood Q, Hegazy H H, Alharthi S and Amin M A 2022 Study of narrow band gap double perovskites $(Sr/Ba)_2BB'O_6$ (B = In, Tl, B' = Sb, Bi) for optical, thermoelectric, and mechanical properties *Materials Today Communication* **31** 103547
[70] Hellman O and Broido D A 2014 Phonon thermal transport in $Bi_2Te_3$ from first principles *Phys. Rev. B* **90** 134309
[71] Campi D, Paulatto L, Fugallo G, Mauri F and Bernasconi M 2017 First-principles calculation of lattice thermal conductivity in crystalline phase change materials: GeTe, $Sb_2Te_3$, and $Ge_2Sb_2Te_5$ *Phys. Rev. B* **95** 024311
[72] Tian Z, Garg J, Esfarjani K, Shiga T, Shiomi J and Chen G 2012 Phonon conduction in PbSe, PbTe, and $PbTe_{1-x}Se_x$ from first principles calculations *Phys. Rev. B* **85** 184303
[73] Sajjad M, Mahmood Q, Singh N and Andreas J 2020 Larsson, ultralow lattice thermal conductivity in double perovskite $Cs_2PtI_6$: a promising thermoelectric material, ACS applied energy *Materials* **3** 11293–9